Shield Construction Effect on the Existing Subway Tunnel Structures and Efficiency of Grouting Reinforcement Measures: a 3D Model and a Case Study

Zhengya ZHANG [1], Bohao LI [2], Yong YAN [3], Jinwei FU [2], Hadi HAERI [4], Vahab SARFARAZI [5*]

[1] *College of Engineering, Zhengzhou Technology and Business University, Zhengzhou 451400, China*
[2] *School of Civil Engineering and Transportation, North China University of Water Resources and Electric Power, Zhengzhou, 450046, China*
[3] *Henan Water Conservancy Investment Group, ZhengZhou 450002, China*
[4] *Department of Mining Engineering, Higher Education Complex of Zarand, Shahid Bahonar University of Kerman, Kerman, Iran*
[5] *Department of Mining Engineering, Hamedan University of Technology, Hamedan, Iran*

http://doi.org/10.5755/j02.ms.41087

Received 7 April 2025; accepted 22 April 2025

The impact of shield construction on existing structures has been analyzed, and the effectiveness of various reinforcement measures has been compared using Midas GTS NX software. This evaluation examines the use of isolation piles and sleeve valve pipe grouting as reinforcement methods to determine their effects on mitigating uneven settlement and horizontal displacement of existing buildings. The analysis reveals that advanced grouting effectively controls the settlement caused by excavation, stabilizing the vertical deformation of the bottom plate within ± 1.5 mm throughout the construction phase. In comparison, in-hole compensation grouting limits this settlement to within ± 1 mm. Additionally, it is observed that in the intersection area of the bottom plate, the reverse bending of the bottom longitudinal beam may result in slight uplift. The results illustrate that the constraints on horizontal displacement provided by isolation piles (walls) and sleeve valve tube grouting were 17.1 % and 38.7 %, respectively, while those on vertical displacement were 32.2 % and 20.1 %, respectively.
Keywords: grouting, settlement, Midas GTS NX software, reinforcement.

1. INTRODUCTION

The rapid population growth in major cities and capitals has significantly driven progress in China's transportation industry. To improve mobility for citizens and reduce commuting times as well as urban traffic congestion, it is essential to construct metro tunnels. One effective method for building these tunnels is shield tunnel construction. However, this technique can lead to surface subsidence, which may affect nearby buildings and structures [1 – 4]. Additionally, subsidence can occur due to earthquakes during or after construction [5 – 7]. Li et al. [8] studied settlement patterns and control measures in constructing tunnels beneath station tracks. Their research used theoretical calculations and numerical simulations to analyze the settlement and displacement of the tunnel-strata-track system, recommending a mix of ground reinforcement techniques to minimize impacts on existing railway tracks. Yang et al. [9] concentrated on the effectiveness of high-pressure jet grouting piles in loess tunnels following water inflow during the operational phase. They used numerical simulations to evaluate the efficacy of this reinforcement strategy and confirmed their results through field monitoring, demonstrating its ability to prevent uplift caused by the softening of surrounding rock. Ma et al. [10] examined how existing pile foundations affect the settlement of suburban stations during tunnel construction. Their simulations highlighted the deformation of structures and optimal pile cutting timings to minimize settlement, emphasizing the role of secondary lining in enhancing tunnel support stiffness. Liu et al. [11] investigated the impact of grouting parameters on slurry diffusion in shallow sand and gravel layers. They found that grouting pressure significantly affects the diffusion radius, while grouting time and water-cement ratio are less important. The study used discrete element software to develop a numerical model for assessing ground settlement from grouting reinforcement. Zhang et al. [12] introduced a high-performance grouting material intended to enhance the support capabilities of anchoring pipes in soft rock tunnels. They conducted tests on mix proportions and strength, identifying critical parameters such as initial setting time and compressive strength. Their field tests proved that using pure cement paste effectively minimizes tunnel settlement and convergence, demonstrating its appropriateness for on-site use Zhou et al. [13] proposed a method to calculate construction disturbance zones in shield tunneling near urban structures. Their case study of the Chengdu Jinxiu Tunnel revealed significant disturbances within the first week of construction and categorized disturbance levels for different structures. They highlighted the use of targeted grouting techniques to reduce vertical settlement in adjacent buildings. Ding et al. [14] developed an enhanced method for estimating grouting quantities in tunnel foundations on

* Corresponding author: V. Sarfarazi
E-mail: *sarfarazi@hut.ac.ir*

anisotropic soft soils. By combining theoretical models with field data, their results highlighted the complexities of soil interactions and the need for integrating nonlinear behaviors, making this method particularly useful for urban tunnel projects in challenging geological conditions Zhang et al. [15] developed a three-dimensional numerical model for tunnel excavation, incorporating initial support hysteresis and validating it with on-site measurements. They identified four stress distribution sections in the pipe-roof and showed that grouting reinforcement can significantly reduce vault settlement in weak geological formations, providing insights into construction parameters affecting tunnel stability. Numerous researchers have examined the settlement and failure of structures caused by construction using finite element numerical methods [16 – 23]. This paper examines the impact of shield construction on existing structures and analyzes how various reinforcement measures influence the response of these structures during the construction of shield tunnels. The innovative aspect of this research lies in demonstrating the effectiveness of isolation piles and sleeve valve pipe grouting in reducing structural displacements during shield construction. The analyses presented utilize quantitative data alongside the innovative application of deformation cloud maps, which enhance the understanding of the construction's effects.

2. SIMULATION OF UNDERPASS REINFORCEMENT

2.1. Compensation grouting in the tunnel

Compensation grouting involves injecting a double-liquid slurry into the soil behind the segment through the segment assembly hole and pre-buried grouting hole, as illustrated in Fig. 1. This process occurs while the shield is excavating and serves multiple purposes: it effectively fills the gap between the segment and the shield tail, allowing for a quick and strong bond between the segment and the surrounding soil. Additionally, it allows for the continuous deepening of the grouting hole, enabling timely grouting to reinforce the soil around the segment. This technique helps mitigate the impact of shield excavation on the existing subway station to some extent.

Grouting slurry concentrations include the cement slurry water-cement ratio, water glass concentration, volume ratio of cement slurry to water glass, and initial setting time. These values are 0.8:1, 25 – 30 C, 2:1, and within 40 seconds, respectively.

Fig. 1. Construction drawings of the secondary grouting site in the hole

During the shield tunneling process, the soil experiences shear deformation and is likely to develop voids and loose areas. These voids, as illustrated in the figure below, can be filled through grouting. This process reduces the porosity of the soil and increases its density, thereby preventing soil settlement.

Additionally, the materials used in grouting can enhance the bearing capacity of the soil once they solidify, allowing it to better withstand the changes in underground stress caused by shield construction. This contributes to minimizing vertical settlement of the station floor that may result from the tunneling process. Fig. 2 illustrates the mechanism of compensatory grouting reinforcement in caves.

Furthermore, grouting creates a degree of cementation within the soil, improving its overall performance. This enhancement helps to disperse and transfer ground stress, reducing local stress concentrations and, consequently, slowing down the settlement of the station floor.

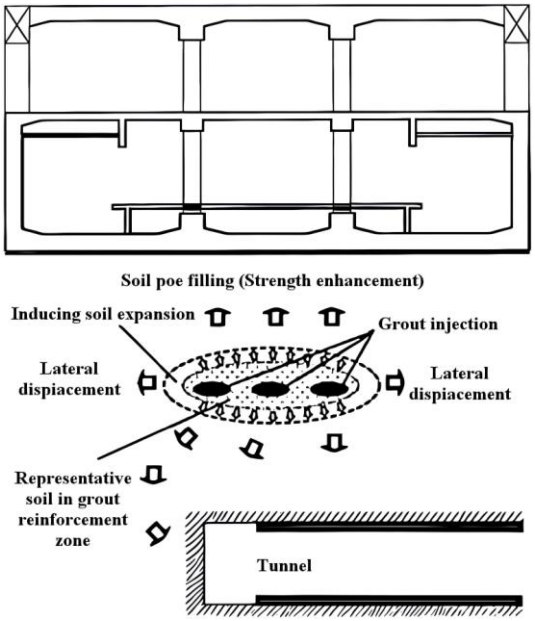

Fig. 2. Mechanism of compensatory grouting reinforcement in caves

The overall model is similar to the unreinforced condition. Fig. 3 illustrates the extent of the grouting reinforcement area, which extends between 9 to 23 steps of excavation on both the left and right lines. The thickness of the grouting body is 1.4 meters, and the elastic modulus of the soil in the grouting reinforcement area is 100 MPa.

Midas GTS NX is a finite element software used in geotechnical engineering, offering modules for static and dynamic analysis, seepage, stress-seepage coupling, consolidation, construction stage analysis, and slope stability. It's widely applied in designing tunnels, slopes, foundation pits, pile foundations, hydraulic projects, and mining. The software features powerful modeling tools and databases, including the ability to generate hybrid meshes, combining hexagonal units for accuracy and tetrahedral units for complex geometries. Fig. 4 illustrates the step-by-step calculations for simulating grouting reinforcement in a hole.

– Initial stress field established: the boundary conditions for the strata are activated, taking into account self-weight and model displacement. The overall static water level is

defined, and zero displacement processing is performed (Fig. 4 a).

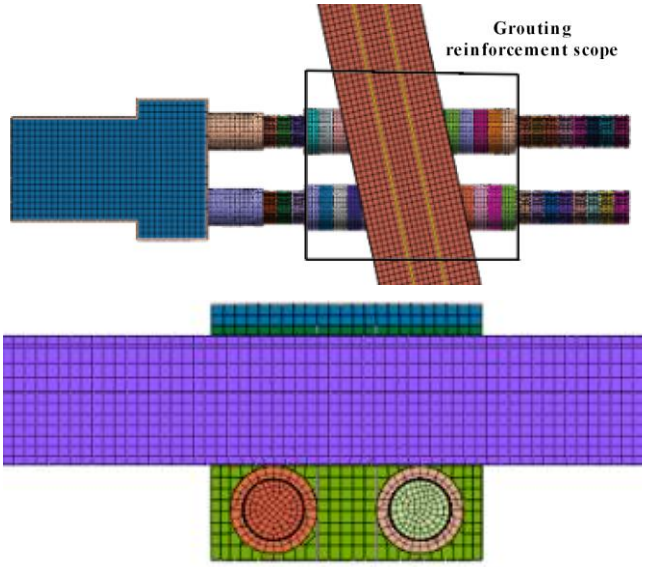

Fig. 3. Schematic diagram of the secondary grouting reinforcement area in the hole

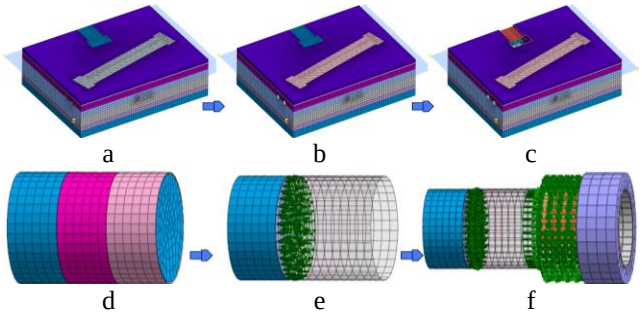

Fig. 4. Simulation steps for borehole grouting reinforcement: a – initial stress field; b – existing subway structures with soil properties deactivated; c – new subway stations with soil excavation; d – left line tunnel S1 excavation; e – left line S2 tunneling with support pressures; f – progress into the reinforced area

– Existing subway stations and tunnels constructed: in the vicinity of the existing subway station (Fig. 4 b), soil properties are deactivated. Structural components such as beams, slabs, and columns of the subway station, along with the backfill properties on the top plate, are activated. Adjustments are made to the properties of the existing tunnel units as necessary.

– New subway stations constructed: soil within the excavation area of the foundation pit for the new subway station is deactivated (Fig. 4 c). Structural components, including beams, slabs, columns, and ground walls of the new station, are activated, followed by zero displacement processing.

– Left line tunnel excavation S1: in the first step of excavation (Fig. 4 d), the original soil within the excavation area is deactivated. The support pressure from the first step excavation soil cabin and the corresponding shield properties for this stage are activated.

– Left line tunneling S2: In the second step of excavation (Fig. 4 e and f), the original soil within the second step excavation area is deactivated. The first step is to excavate soil chamber support pressure and the properties of the first step shield shell are reactivated. The second step, excavation soil chamber support pressure and shield tail grouting pressure are activated. The assembly of segments in this excavation step is completed, and thrust is applied to the segments. Following a delay, the shield tail grouting layer and the secondary grouting unit properties are activated while the grouting pressure is deactivated.

– Left line excavation to the reinforcement area: when section S26 is reached during excavation, the soil properties of the horizontal freezing reinforcement area will be activated as the left line approaches the end well. The unit properties will be modified until the left line tunnel excavation process is completed.

– Right line excavation: when step S29 is reached during the left line excavation, the right line excavation will begin. The same methodology used for the left line will be followed for the right line excavation until the double line excavation is completed.

2.2. Advance duct grouting

The advanced grouting scheme for the shield machine involves installing a grouting pipe at the front, where slurry is injected to create a solid grouting curtain that stabilizes the surrounding ground. Simulations show that the advanced grouting rod should be 16 m long, with an effective range of about 10 m in front of the cutterhead.

The minimum vertical clearance between the tunnel excavation area and the existing station floor is 1.475 m, allowing a maximum reinforcement height of 1.45 m above the tunnel vault. The grout outlet height typically does not exceed 2 m above the tunnel. When the shield machine reaches this point, reinforcement of the upper soil is significantly improved. The drill rod arrangement is shown in Fig. 5.

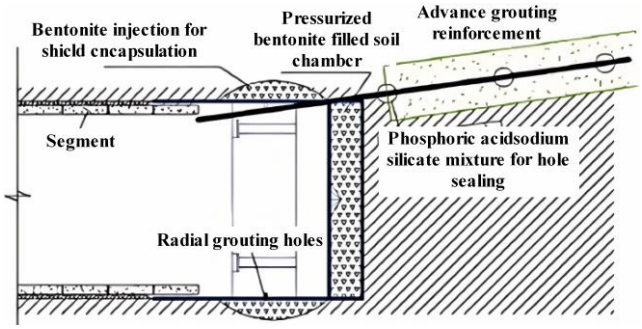

Fig. 5. Overrun grouting drill pipe arrangement

To achieve advanced grouting, a grouting hole with a diameter of 100 mm is designed on the shield body. This hole is drilled using a drill bit and drill rod with a diameter of 42 mm. Each section of the drill rod is 2.0 m long, and a grouting channel is incorporated inside the drill rod. The drill rod connects to the grouting port on the shield body via a flange, as illustrated in Fig. 6. The segmented backward advance grouting method is a technique for soil reinforcement. It involves drilling a hole into the soil, mixing two liquids (liquid A and liquid B) to create a slurry, and then delivering this slurry to the bottom of the hole through pipes and drill rods. Double-liquid grouting is performed at a designated volume and pressure, which

induces cracks and deformation in the soil, allowing the slurry to fill these voids and enhance the soil's stability.

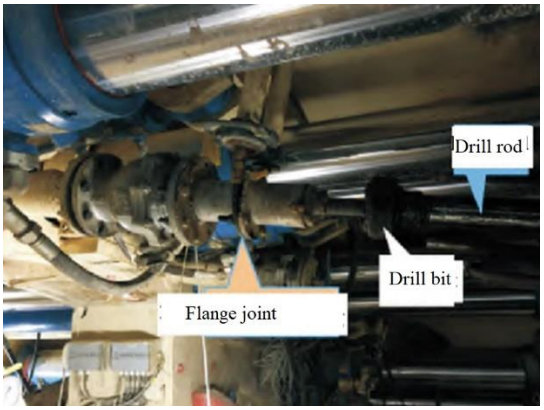

Fig. 6. Drill pipe and shield connection method

After grouting one section of the hole, the drill rod is lifted a certain distance before proceeding to the next section of grouting. The working process is illustrated in Fig. 7.

The overall model resembles the unreinforced condition. Considering that the minimum vertical clearance between the tunnel excavation area and the existing station floor is 1.475 meters, the thickness of the reinforcement area has been set at 1.4 meters, with an elastic modulus of 100 MPa.

In Fig. 8, a step-by-step calculation of the simulation for overrun grouting reinforcement is shown.

– Establish the initial stress field (Fig. 8 a): the boundary conditions of the strata are activated, self-weight is accounted for, displacement is modeled, the overall static water level is defined, and zero displacement processing is performed.

– Construction of existing subway stations and tunnels (Fig. 8 b): the soil within the area of the existing subway station is deactivated. Structural units such as beams, slabs, and columns of the existing subway station are activated. Backfill properties on the top plate are activated, and modifications are made to the properties of the existing tunnel units.

– Construction of new subway stations (Fig. 8 c): the soil within the excavation area of the foundation pit for the new subway station is deactivated. Structural units, including beams, slabs, columns, and ground walls of the new station, are activated, and zero displacement processing is performed.

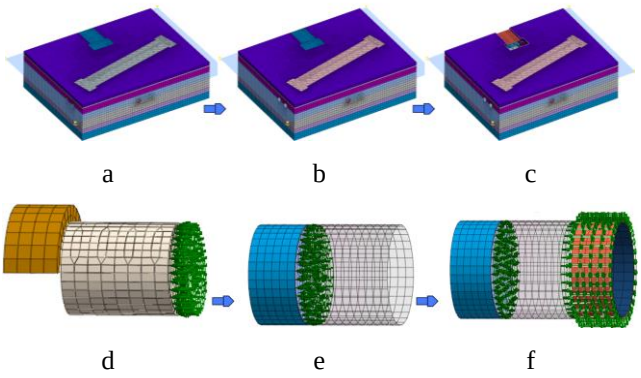

Fig. 8. Simulation of overrun grouting reinforcement: a – initial stress field setup; b – deactivation of soil properties for existing subway structures; c – activation of new subway station units; d – excavation of left line S1; e – excavation of left line S2 with support pressures; f – progression into horizontal freezing reinforcement area

– Left line excavation S1 (Fig. 8 d): the original soil in the first step excavation area is deactivated, and the support pressure and shield properties for this stage are activated. Advanced reinforcement soil above the cutterhead is modified.

– Left line excavation S2 (Fig. 8 e and f): the original soil in the second step is deactivated, along with the first step's support pressure and shield properties. The second step, support pressure and shield tail grouting pressure are activated. Segment assembly is completed, and thrust is applied, with a delay in activating the shield tail grouting layer.

– Left line excavation: upon reaching S26, soil properties for horizontal freezing in the reinforcement area are activated as the left line nears the end well. Adjustments are made until the left line tunnel excavation is complete.

– Right line excavation: The right line excavation starts at S29, mirroring the left line process until both lines are fully excavated.

Fig. 9 illustrates the cumulative vertical displacement of the base plate under compensatory grouting reinforcement. As illustrated in Fig. 9, when the left-line shield was excavated toward the front of the station, a slight underpressure in the soil compartment caused the existing subway station floor near the cutter head to experience an initial vertical displacement, reaching a maximum settlement of 0.51 mm.

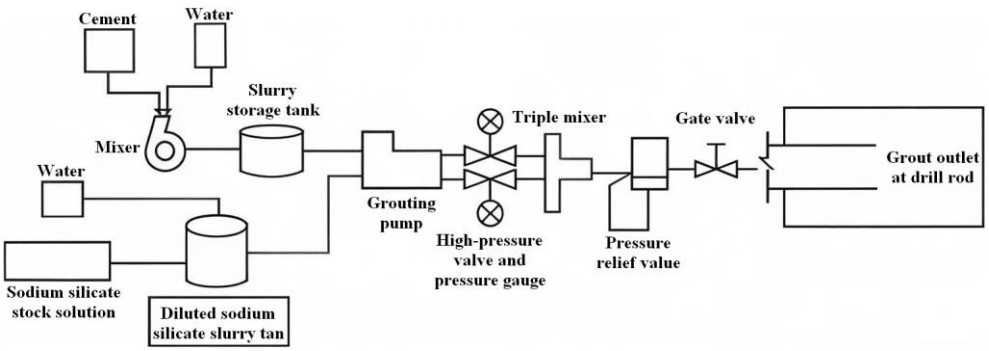

Fig. 7. Grouting flow chart

3. COMPARATIVE ANALYSIS OF REINFORCEMENT MEASURES

3.1. Cumulative settlement analysis of the bottom plate

At the point where it passed through the center of the station floor, the maximum vertical settlement was recorded at the projection of the left-line center axis on the floor, which measured 1.05 mm. Following the completion of the left-line excavation, the location of the maximum vertical settlement shifted as the excavation progressed, with a recorded value of 0.95 mm.

When the right-line shield was excavated toward the front of the station, the maximum vertical displacement on the floor was still aligned with the projection line extending from the left-line center axis to the floor. However, the advanced vertical settlement caused by the right-line excavation resulted in a maximum vertical displacement of 0.96 mm. As the right-line face passed through the middle of the floor, the reverse bending of the bottom longitudinal beam reduced the impact of the left-line's passage on the vertical deformation of the floor, resulting in a maximum vertical displacement of 0.89 mm. Once the right-line excavation was completed, the maximum vertical settlement of the floor was stabilized at 0.93 mm. As illustrated in Fig. 10, under the advanced grouting reinforcement condition, a grouting curtain formed in the upper soil in front of the face reduced the advanced vertical settlement due to the left line excavation near the underpass to 0.23 mm. When the left line shield progressed to the middle of the bottom plate, the vertical settlement increased to 1.39 mm. After the completion of the left line excavation, the settlement displacement reached 1.46 mm. During the excavation of the right line, vertical settlement also occurred at the bottom plate projection's center, which intensified the disturbance caused by the left line underpass when compared to the secondary grouting reinforcement condition. Upon completing the right line excavation, the maximum vertical settlement of the bottom plate stabilized at 1.51 mm.

3.2. CUMULATIVE DISPLACEMENT ANALYSIS OF MONITORING POINTS

For a quantitative analysis, monitoring lines and points were established at the bottom plate.

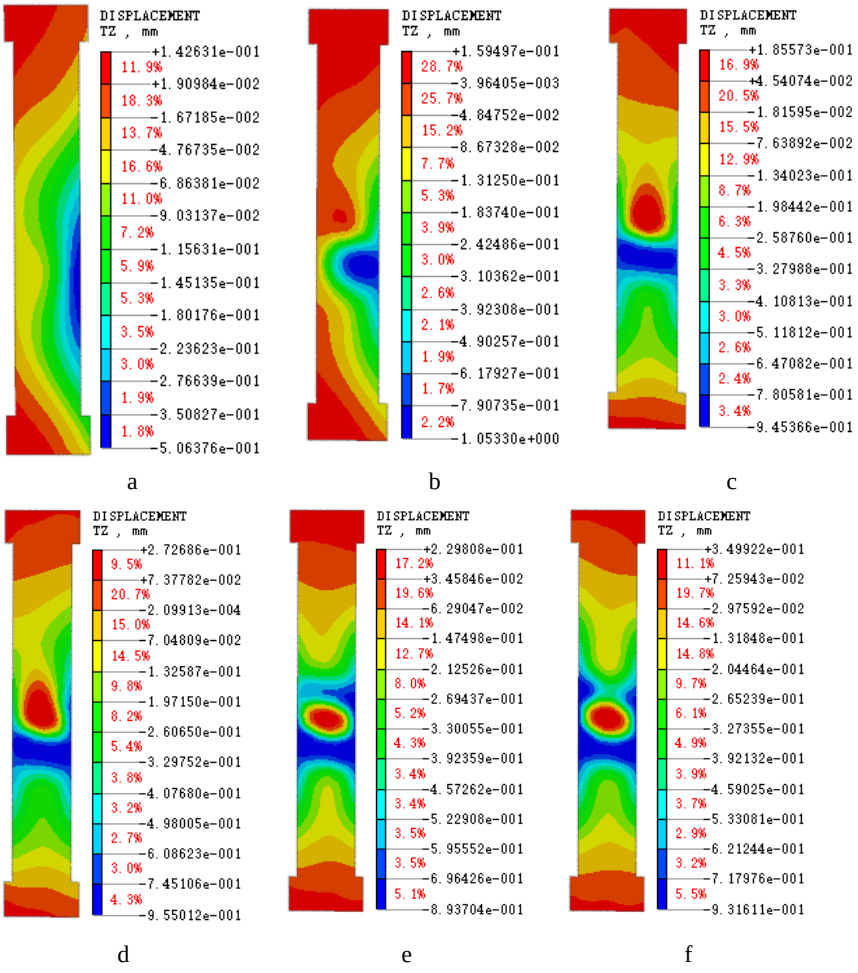

Fig. 9. Cumulative vertical displacement of the base plate during compensatory grouting at key stages: a – before the left line passes beneath; b – left line under the middle of the floor; c – left line excavation complete; d – before the right line passes beneath; e – right line under the middle of the floor; f – right line excavation complete

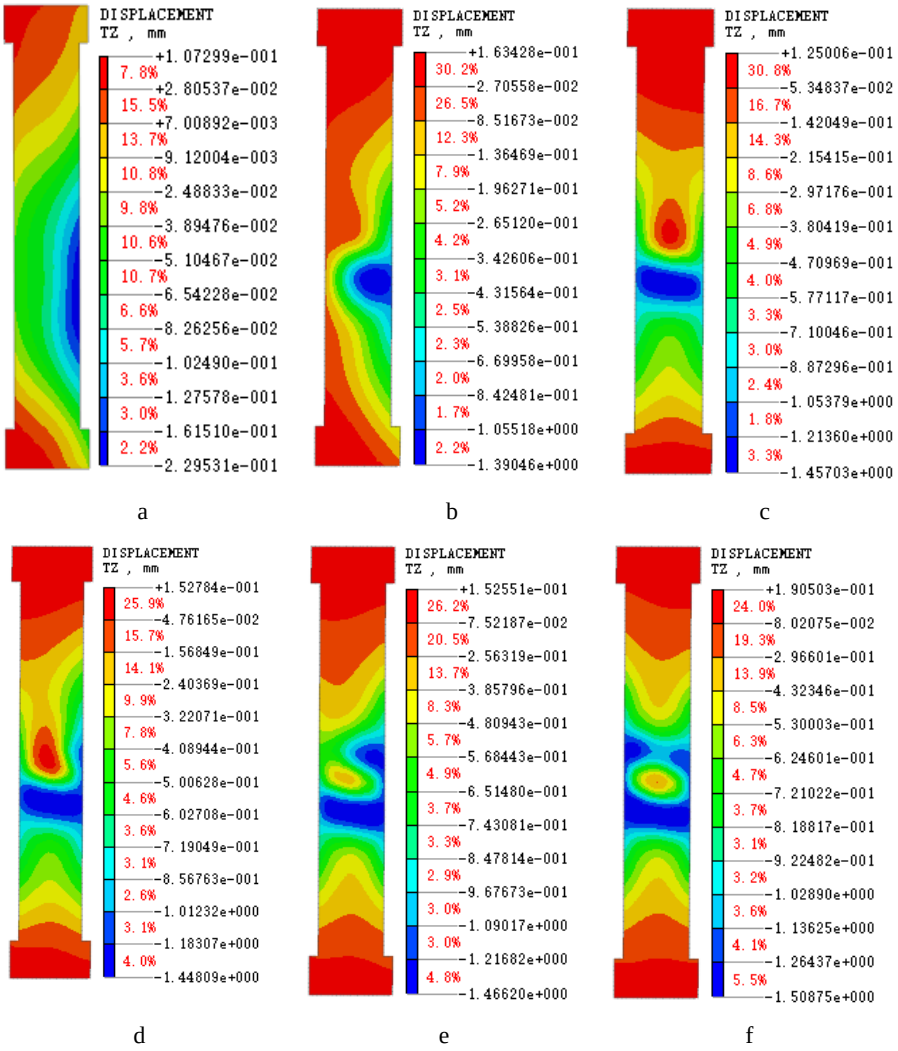

Fig. 10. Cloud view of cumulative vertical displacement of the base plate during overtopping grouting at critical stages: a – before the left line passes beneath; b – left line under the middle of the floor; c – completion of left line excavation; d – before the right line passes beneath; e – right line under the middle of the floor; f – completion of right line excavation

The monitoring line runs along the longitudinal center of the bottom plate, with the measurement point positioned at the center of the projection of the central axis of the two tunnels on the bottom plate, as shown in Fig. 11.

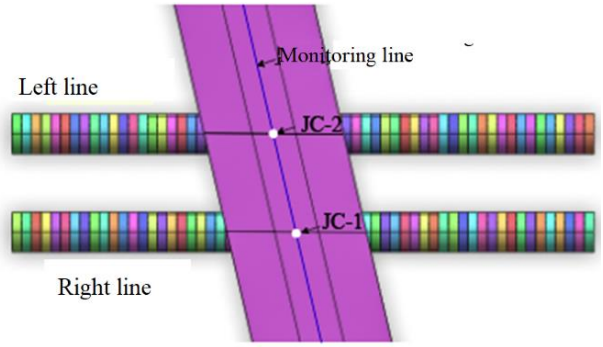

Fig. 11. Schematic of monitoring locations

Fig. 12 illustrates the distribution curve of the vertical displacement along the monitoring line, with the center of the double line serving as the axis of symmetry. The figure indicates that the vertical deformation of the bottom plate is greatest under unreinforced conditions. Additionally, due to the reverse bending of structures like the bottom plate beam, the vertical settlement displacement in the projection area at the center of the double line on the bottom plate shows a negative growth trend. With the implementation of reinforcement measures such as advanced grouting and secondary grouting, the vertical deformation of the bottom plate has been partially mitigated. Among these measures, secondary grouting exhibits the most significant effect in reducing the displacement of the station's bottom plate, effectively controlling the vertical displacement to within ±1 mm.

Fig. 13 illustrates the cumulative vertical displacement curve of the JC-1 measuring point. As the shield tunneling progresses, the cumulative displacement at this measuring point continues to change, exhibiting a positive correlation with the displacement evolution trends under different working conditions. During stage B, the cumulative settlement at the measuring point reached its maximum values under various working conditions, specifically 1.97 mm, 1.61 mm, and 1.09 mm, respectively. After stage E, the displacement trend stabilized due to the structural

deformation coordination capabilities of the overall system of the station.

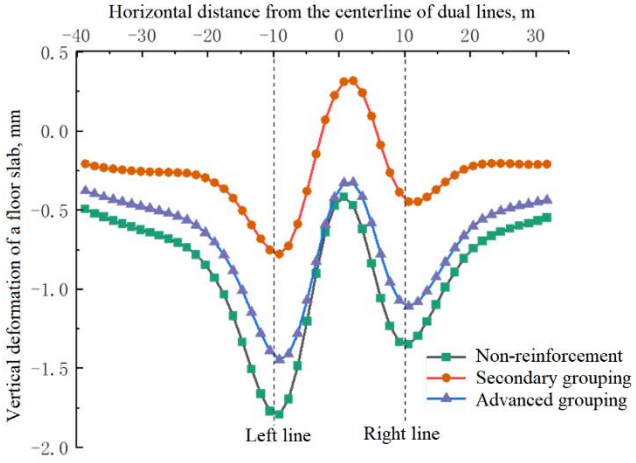

Fig. 12. Cumulative vertical displacement curve of the monitoring line of the bottom plate completed by double line boring

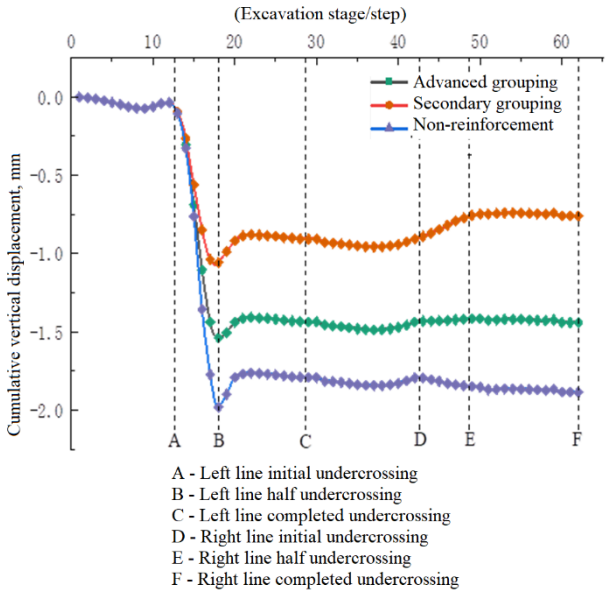

Fig. 13. The cumulative vertical displacement curve of the JC-1 measuring point

Fig. 14 illustrates the cumulative vertical displacement curve for the JC-2 measuring point. Following stage A, the left line experiences secondary grouting reinforcement, causing the measuring point to bulge due to the reverse bending effect. After reaching stage D, the measuring point begins to settle gradually. In stage E, the cumulative vertical displacement at this measuring point reaches its maximum values of 1.84 mm, 1.25 mm, and 0.63 mm under different working conditions. After stage E, the displacement trend stabilizes due to the deformation coordination capability of the overall structure of the station.

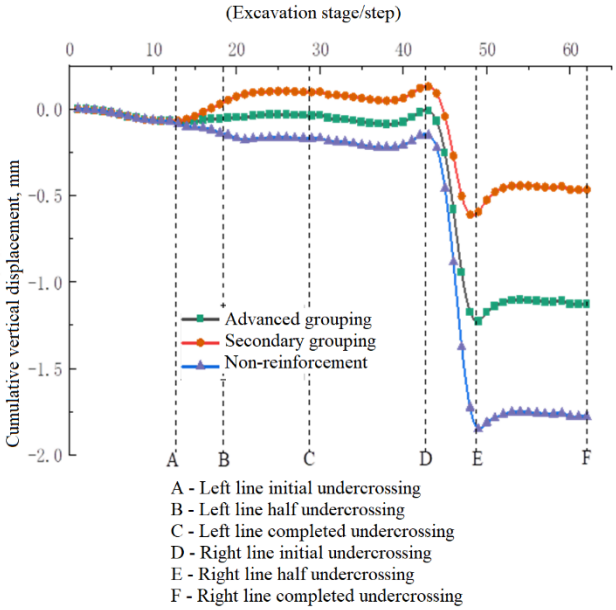

Fig. 14. Cumulative vertical displacement curve at measurement points (JC-2)

3.3. ANALYSIS OF THE STRESS AND DEFORMATION CHARACTERISTICS OF THE BOTTOM LONGITUDINAL BEAM

As illustrated in Table 1, the secondary grouting reinforcement in the tunnel resulted in a maximum vertical settlement of 0.93 mm and a horizontal displacement of 0.4 mm for the bottom longitudinal beam.

Table 1. Bottom longitudinal beam deformation and force conditions

Working conditions	Stage	Maximum vertical settlement, mm	Maximum horizontal displacement, mm	Maximum bending moment, kN·m
Secondary Grouting	Before the left line passes under the bottom	0.15	0.10	1828.3
	The left line passes under the bottom to the middle of the bottom	0.78	0.02	1988.1
	The left line passes under the bottom	0.88	0.23	2275.5
	Before the right line passes under the bottom	0.93	0.27	2278.5
	The right line passes under the bottom to the middle of the bottom	0.87	0.29	2287.7
	The right line passes under the bottom	0.78	0.40	2298.6
Advance Grouting	Before the left line passes under the bottom	0.11	0.09	1819.4
	The left line passes under the bottom to the middle of the bottom	0.97	0.01	2018.1
	The left line passes under the bottom	1.38	0.30	2345.1
	Before the right line passes under the bottom	1.39	0.31	2348.4
	The right line passes under the bottom to the middle of the bottom	1.43	0.33	2359.5
	The right line passes under the bottom	1.44	0.45	2367.8

The maximum bending moment was recorded at 2298.6 kN·m, demonstrating effective reinforcement. In contrast, under the advanced grouting reinforcement, the bottom longitudinal beam experienced a maximum vertical settlement of 1.44 mm and a horizontal displacement of 0.45 mm, which occurred when the right line was completed and passed beneath. The maximum bending moment in this case was 2367.8 kN·m, indicating that this reinforcement also provided some benefit.

4. CONCLUSIONS

This paper examines the area under Huanghe South Road Station of Line 1, presenting a case study for a supporting project. A three-dimensional model using the stratum-structure method has been developed, detailing the excavation process. Grouting and other techniques simulate strata loss, allowing for the creation of deformation cloud maps of the stratum and station structure. The analysis of various reinforcement measures leads to key conclusions.

1. When compared to the response of shield construction on buildings without reinforcement measures, the constraints on horizontal displacement by isolation piles (walls) and sleeve valve tube grouting were 17.1 % and 38.7 %, respectively. The constraints on vertical displacement were 32.2 % and 20.1 %, respectively.
2. The effect of isolation piles (walls) on vertical displacement of frame structures and pile foundations was superior to that of sleeve valve tube compensation grouting, while the opposite was true for horizontal displacement.
3. Isolation pile (wall) reinforcement demonstrated better control over the maximum axial force of columns, whereas sleeve valve tube compensation grouting provided superior control over the maximum bending moment of beams. Both methods effectively managed the inclination of buildings.
4. The advance grouting measure can efficiently create a grouting curtain in the upper soil ahead of the cutterhead, significantly reducing settlement caused by shield tunneling. Secondary grouting effectively reinforces the soil around the tunnel and between the tunnel and the bottom plate.
5. After the tunneling is completed, the projection area at the center of the double lines on the bottom plate is slightly raised. Both construction schemes effectively control the deformation of the bottom plate and the stress on the bottom longitudinal beam, keeping the maximum displacement of the bottom plate within 1.5 mm and 1 mm, respectively.
6. The feasibility of the proposed 3D model is highlighted in the evaluation and visualization of the suggested reinforcement techniques. The advantages of both isolation piles (walls) and sleeve valve tube grouting can be assessed within the context of specific projects using this model.

Acknowledgments

This work was supported by National Natural Science Foundation of China (No. 52479100), National Foreign Experts Program of China (No. S20240157 and No. H20240271), and Outstanding Foreign Scientist Studio of Henan Province (No. GZS2025015).

REFERENCES

1. **Kasper, T., Meschke, G.** A Numerical Study of the Effect of Soil and Grout Material Properties and Cover Depth in Shield Tunnelling *Computers and Geotechnics* 33 2006: pp. 234 – 247. https://doi.org/10.1016/j.compgeo.2006.04.00
2. **Zhang, Z.G., Zhang, Z.X., Jiang, Y.J., Bai, Q.M., Zhao, Q.H.** Analytical Prediction for Ground Movements and Liner Internal Forces Induced by Shallow Tunnels Considering Non-Uniform Convergence Pattern and Ground-Liner Interaction Mechanism *Soils and Foundations* 57 2017: pp. 211 – 226. https://doi.org/10.1016/j.sandf.2017.03.004
3. **Wang, H.L., Ge, J.J., Wang, M., Jiang, Y.X., Feng, S., Li, Y.D., Ran, L., Jin, T.** Study on the Influence of Secondary Grouting on Soil Settlement Above Shield Tunnel. In: Feng, G. (eds) Proceedings of the 10th International Conference on Civil Engineering. ICCE 2023. Lecture Notes in Civil Engineering, 526. Springer, Singapore 2024. https://doi.org/10.1007/978-981-97-4355-1_35
4. **Ding, Z., He, S.Y., Zhou, W.H., Xu, T., He, S.H., Zhao, X.** Analysis of Ground Deformation Induced by Shield Tunneling Considering the Effects of Muck Discharge and Grouting *Transportation Geotechnics* 30 2021: pp. 00629. https://doi.org/10.1016/j.trgeo.2021.100629
5. **Shats'kyi, I.P., Struk, A.B.** Stressed State of Pipeline in Zones of Soil Local Fracture *Strength of Materials* 41 2009: pp. 548 – 553. https://doi.org/10.1007/s11223-009-9165-9
6. **Bulat, A.F., Dyrda, V.I., Grebenyuk, S.N., Agal'tsov, G.N.** Methods for Evaluating the Characteristics of the Stress-Strain State of Seismic Blocks under Operating Conditions *Strength of Materials* 51 2019: pp. 715 – 720. https://doi.org/10.1007/s11223-019-00129-x
7. **Wan, Z., Cao, W., Jiang, P.H., Liu, Y.Y.** Analytical Solution of Cylindrical Cavity Expansion in the Construction Process of Pipe Pile *Strength of Materials* 55 2013: pp. 426 – 440. https://doi.org/10.1007/s11223-023-00536-1
8. **Li, P., Lu, F., Huang, H., Qiu, W.** Railway Track Settlement Patterns and Control Measures for Multi-Tunnel Construction Underneath a Station Track Group: A Case Study *Scientific Reports* 14 2024: pp. 14474. https://doi.org/10.1038/s41598-024-64916-6
9. **Yang, Z., Dai, J., Wang, Q., Tian, X., Liu, H.** Analysis of Reinforcement Effect of High Pressure Jet Grouting Pile During Water Inflow of Loess Tunnel Basement During Operation Period. In: Bieliatynskyi, A., Komyshev, D., Zhao, W. (eds) Proceedings of Conference on Sustainable Traffic and Transportation Engineering in 2023. CSTTE 2023. Lecture Notes in Civil Engineering, 603. Springer, Singapore 2024. https://doi.org/10.1007/978-981-97-5814-2_31
10. **Ma, B., Wu, S., Chen, Q., Liang, E., Li, X.** The Influence of Existing Piles on Station Settlement during the Construction of a Tunnel Undercrossing under Existing Stations *Scientific Reports* 14 2024: pp. 14024. https://doi.org/10.1038/s41598-024-63921-z
11. **Liu, S., Xie, Z., Zhang, J., Sun, J., Tian, Q., Yu, Z., An, X., Wu, W.** Experimental Study on the Diffusion Law of

Horizontal Grouting in Shallow Sand Gravel Layer *KSCE Journal of Civil Engineering* 28 2024: pp. 3192 – 3207. https://doi.org/10.1007/s12205-024-1744-6

12. **Zhang, L., Chen, J., Chen, L., Luo, Y., Liu, W., Dong, F., Chen, H., Zhu, H.** Development and Application of High-Performance Grouting Materials for Anchoring Pipe in Soft Rock Tunnel *KSCE Journal of Civil Engineering* 27 2023: pp. 4494 – 4507. https://doi.org/10.1007/s12205-023-0459-4
13. **Zhou, Z., Guo, F., Ni, J., Feng, K., Zhang, J., Liu, Y.** Research on the Method of Construction Disturbance Zoning for Shield Tunnel Approaching to Urban Structures *Frontiers of Structural and Civil Engineering* 18 2024: pp. 1663 – 1679. https://doi.org/10.1007/s11709-024-1109-8
14. **Ding, B., Lou, P., Huang, C., Li, W., Wang, Y.** Investigating Grouting Body Nonuniform Expansion in Anisotropic Underground Soil Mechanics *Scientific Reports* 14 2024: pp. 32004. https://doi.org/10.1038/s41598-024-83492-3
15. **Zhang, X., Zhang, D., Rong, Y., Ma, Y., Yao, C., Sun, Y.** Study on the Stability of Tunnel in Weak Surrounding Rock Considering Initial Support Parameters and Excavation Method *KSCE Journal of Civil Engineering* 28 2024: pp. 2427 – 2439. https://doi.org/10.1007/s12205-024-1520-7
16. **Nguyen, N.T., Nguyen, T.T.T., Tran, A.D.** Assessing the Spatial Variability of Compressive Strength of In-Situ Concrete: From Laboratory to Construction Site *Strength of Materials* 54 2022: pp. 918 – 928. https://doi.org/10.1007/s11223-022-00468-2
17. **Yang, Y., Cheng, H., Fu, J., Haeri, H., Hou, R.**. Numerical Investigation of Stress and Strain Analysis in Rock Breaking of TBM Disk Cutters *Strength of Materials* 56 2024: pp. 209 – 221. https://doi.org/10.1007/s11223-024-00640-w
18. **Sekban, D.M., Yaylacı, E.U., Özdemir, M.E., Yaylacı, M., Tounsi, A.** Investigating Formability Behavior of Friction Stir-Welded High-Strength Shipbuilding Steel using Experimental, Finite Element, and Artificial Neural Network Methods *Journal of Material Engineering and Performance* 34 2024: pp. 4942–4950. https://doi.org/10.1007/s11665-024-09501-8
19. **Fuyad, S.T.M., Al Bari, Md.A., Makfidunnabi, Md., Nain, H.M.Z., Özdemir, M.E., Yaylaci, M.** Finite Element Analysis of Ratcheting on Beam under Bending-Bending Loading Conditions *Structural Engineering and Mechanics* 89 (1) 2024: pp. 023 – 031. https://doi.org/10.12989/sem.2024.89.1.023
20. **Srivastav, S., Chawla, S., Mishra, S.** Numerical Analysis of Moving Train Induced Vibrations on Tunnel, Surrounding Ground and Structure *Earthquake Engineering, Vibration* 23 2024: pp. 179 – 192.34 https://doi.org/10.1007/s11803-024-2223-2
21. **Tian, Z., Zhang, Z., Zhang, G., Shan, X., Liu, W.** Impact Analysis of Tunnel Crossing Pile Foundation at Different Angles *Scientific Reports* 15 2025: pp. 4770. https://doi.org/10.1038/s41598-024-83863-w
22. **Aktarer, S.M., Küçükömeroğlu, T., Sekban, D.M., Yaylaci, E.U., Yaylaci, M., Özdemir, M.E., Mirzaloglu, İ.** Analysis of the Changes in Microstructure, Mechanical, and Contact Properties of Multi-Pass Friction Stir Processed DP800 Steel *Advances in Nano Research* 18 (3) 2025: pp. 253 – 264. https://doi.org/10.12989/anr.2025.18.3.253
23. **Yaylacı, M., Yazıcıoğlu, A., Yaylacı, E.U., Terzi, M., Birinci, A.** Evaluation of the Contact Problem of Two Layers, One of Functionally Graded, Loaded by Circular Rigid Block and Resting on a Pasternak Foundation by Analytical and Numerical (FEM and MLP) Methods *Archive of Applied Mechanics* 95 2025: pp. 75. https://doi.org/10.1007/s00419-025-02787-7